Portraying the Hosts: Stellar Science From Planet Searches

Bárbara Rojas-Ayala[1], Isabelle Boisse[2], Philip S. Muirhead[3], , Alexander Binks[4], Jason A. Dittmann[5], Jean-François Donati[6], Scott W. Fleming[7,8], Anna-Lea Lesage[9], Julien Morin[10], Stefanie Raetz[11], Jennifer C. Yee[5]

[1]*Instituto de Astrofísica e Ciências do Espaço, Universidade do Porto, CAUP, Rua das Estrelas, PT4150-762 Porto, Portugal*

[2]*Aix Marseille University, CNRS, LAM (Laboratoire d'Astrophysique de Marseille) UMR 7326, 13388, Marseille Cedex 13, France*

[3]*Department of Astronomy, Boston University, 725 Commonwealth Avenue, Boston, MA 02215, USA*

[4]*Astrophysics Group, Keele University, Staffordshire ST5 5BG, UK*

[5]*Harvard-Smithsonian Center for Astrophysics, 60 Garden St., Cambridge, MA, 02138*

[6]*Université de Toulouse / CNRS-INSU, IRAP / UMR 5277, Toulouse, F–31400 France*

[7]*Space Telescope Science Institute, 3700 San Martin Dr, Baltimore, Maryland, 21218 USA*

[8]*Computer Sciences Corporation, 3700 San Martin Dr, Baltimore, Maryland, 21218 USA*

[9] *Leiden Observatory, Leiden University, Niels Bohrweg 2, 2333CA, Leiden, The Netherlands*

[10]*Université Montpellier / CNRS-INSU, LUPM / UMR 5299, 34095 Montpellier, France*

[11]*European Space Agency, ESTEC, SRE-S, Keplerlaan 1, 2201 AZ Noordwijk, The Netherlands*

Abstract. We present a compendium of the splinter session on stellar science from planet searches that was organized as part of the Cool Stars 18 conference. Seven speakers discussed techniques to infer stellar information from radial velocity, transit

and microlensing data, as well as new instrumentation and missions designed for planet searches that will provide useful for the study of the cool stars.

1. Motivation

The discovery of new worlds has driven efforts to characterize in detail the properties of their host stars. For a given planet-hosting star, we want to know its size, mass, age, effective temperature, metallicity, activity cycle, distance from us, and any other physical features that would aid in understanding the corresponding planetary system. Fortuitously, much of the characterization can be done using the same data that enabled the initial planet discoveries. The spectra obtained from radial velocity (RV) surveys, and the photometry and imaging data from transit and microlensing surveys, contain a wealth of information about the host stars' atmospheres, interiors and prior evolution.

The goal of this splinter session was to highlight and review some of the results concerning stellar science from the past 20 years of planet surveys and to promote dialogue to encourage new ideas about existing and future planet survey data. This article is a compendium of all the splinter presentations and provides concrete examples of the stellar information that can be inferred from RV, transit and microlensing data, as well as information about new instruments and missions that will enrich our understanding of cool stars. The following sections were provided by each of the speakers and are a summary of their presentations in the order they were presented during the session. A video of the session is available in the webpage of the splinter[1].

2. Stellar Activity Features Seen From Planet Search Data - Isabelle Boisse

Most of the exoplanet science is dependent on the stellar knowledge. One of them that has to be understood is the magnetic activity when we search for planets with radial velocity or photometry measurements. The main shape of stellar activity and spots properties have to be understood, for example, to choose the best targets to search for low-mass planets in the habitable zone or to derive the accurate parameters of a planetary system. With that aim, we will try to review in this presentation how these studies lead to give clues on several activity features that were not previously observable on Sun-like stars.

3. Trigonometric Parallaxes and the Inferred Properties for 1507 mid-to-late M-dwarfs from the MEarth Planet Survey - Jason A. Dittmann[2]

The MEarth survey has been actively searching for small rocky planets around the smallest, nearest stars to the Sun. Over this time we have taken more than two million images of approximately 1700 mid-to-late M dwarf stars in the northern hemisphere. Prior to our

[1] https://sites.google.com/site/portrayingthehostscs18/

[2] with J. M. Irwin (CfA), D. Charbonneau (CfA), Z. K. Berta-Thompson (MIT)

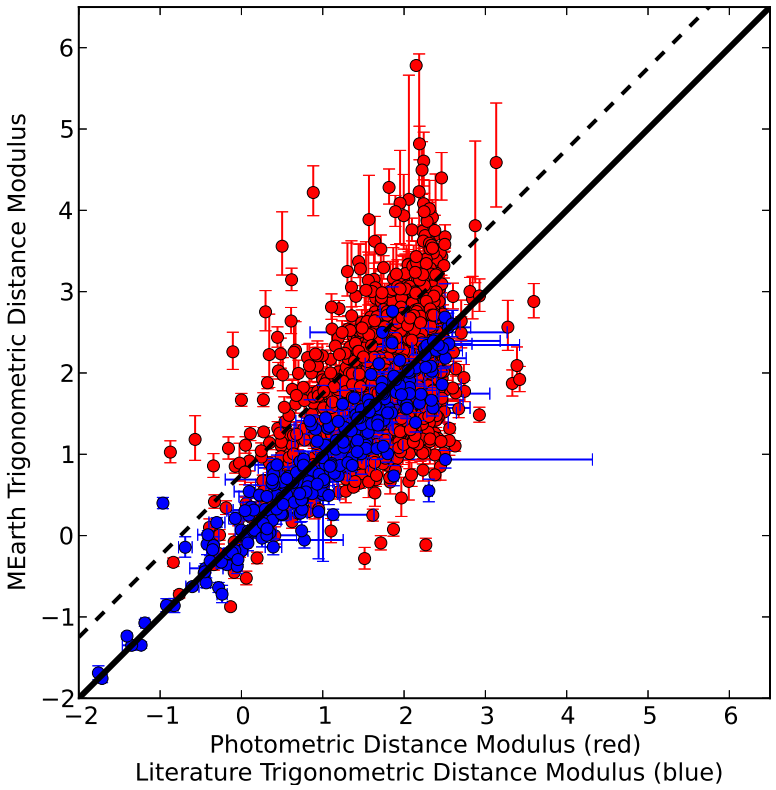

Figure .1: Plot of the MEarth distance modulus versus the expected distance modulus from either previous literature measurements (blue) or the piece-wise linear V-J fit from Lépine (2005) (red). Unresolved equal mass binaries should fall on the dashed line. We note that the MEarth astrometric result is consistent with previous parallax studies and has a much lower dispersion than photometric estimates.

results, most of our stars were characterized solely with data from photographic plates. The data provided by the MEarth survey has allowed us to discover and characterize eclipsing binary systems, measure short and long term rotation periods of stars, and directly measure the distances to these stars via trigonometric parallaxes. In this talk, I will discuss the MEarth Observatory, how it operates, and then discuss MEarthś recent contributions to our understanding of low mass stars. Specifically, I will describe the astrometric pipeline we have developed to measure the trigonometric parallaxes to 1507 systems with a typical accuracy of 4 milliarcseconds and how we have used these results to more reliably estimate the stellar mass and stellar radii for these stars. I will further discuss recent work in calibrating the MEarth photometric system with nightly standard field observations and our progress in obtaining precise broadband optical magnitudes for these stars. We use these results to derive new photometric estimates of distance and metallicities. Finally, I will outline our future plans for the MEarth Observatory and the newly online MEarth South observatory at CTIO.

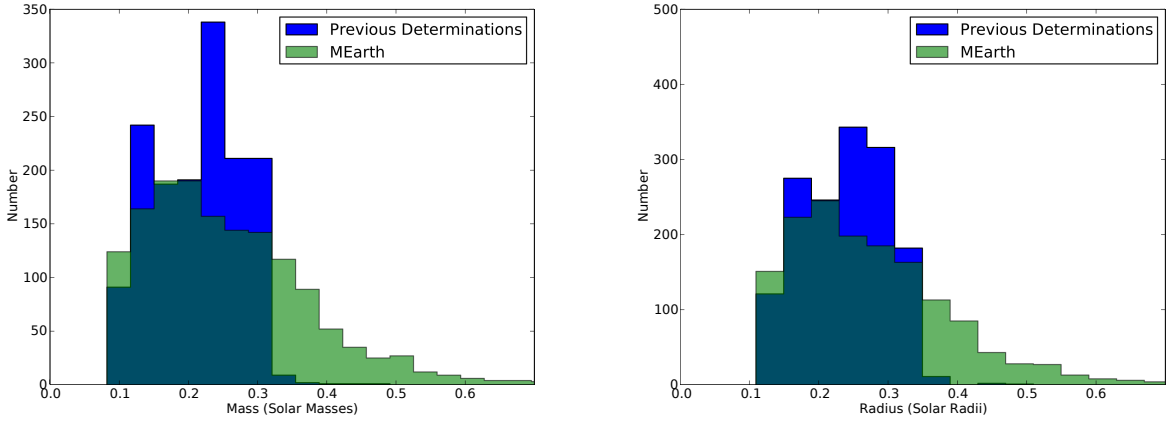

Figure .2: Left: Histogram of the distribution of stellar masses of the MEarth target stars based on our previous photometric determinations (blue, Nutzman & Charbonneau (2008)) and based on the absolute K magnitude derived from the MEarth astrometric data and the 2MASS survey (green). We find the peak of our distribution shifts towards smaller mass stars but there is a significant long tail of stars with higher masses (due to being further away) than previously estimated. We note that at the extremely high mass end ($M >\sim 0.75 M_{\odot}$), the Delfosse et al. (2000) relation is no longer accurate, and that stars in this region are likely to be unresolved binaries, as color information makes them unlikely to be earlier type stars. Right: Identical, but transforming mass to radius with the relation published by Bayless & Orosz (2006).

3.1 Trigonometric Parallaxes from the MEarth Photometric Survey

The MEarth Observatory is an array consisting of 8 identical f/9 40 cm Ritchey-Chrétien telescopes on German equatorial mounts at the Fred Lawrence Whipple Observatory on Mount Hopkins, Arizona and operate every clear night from September through July. Recently, we have commissioned an identical array in the Southern hemisphere at Cerro Tololo, Chile. As MEarth has taken a large number of images of its target stars over the course of entire observing seasons, we investigated whether the MEarth images themselves could be used to measure the trigonometric parallax distances to our targets. We found that the MEarth images are well-suited for astrometric analysis and modified our survey to provide astrometric measurements of all of our stars every 10 days. Here we present the results of this study and trigonometric distance measurements for 1507 stars. For a detailed description of our data reduction and astrometric analysis, as well as our catalog, please see our published paper in Dittmann et al. (2014)

In Figure .1, we show the distance modulus as expected from the photometric distance, using the calibration from Lépine (2005), compared to the value derived from the MEarth astrometry, as well as stars that have previous trigonometric parallax determinations available. In this plot, an equal mass binary would have an offset of 0.75 in distance modulus from the photometric distance modulus estimate. Utilizing these results, we can more accurately estimate the stellar parameters of these stars. Delfosse et al. (2000) obtained an empirical

relation between the masses of low mass stars and their luminosities in the near infrared in the K band. We have used our trigonometric parallax results, combined with available K-band photometry to reevaluate the masses and radii of these stars. In Figure .2, we show histograms of our newly derived stellar masses and radii compared to the values derived by Nutzman & Charbonneau (2008), which used the photometric distance measurement and the same mass-radius relationship. For stars where the newly estimated mass is $M < 0.5 M_{\odot}$, we find a median of the absolute value of the offset of $\Delta M \approx 0.08 M_{\odot}$, whereas if we take the global sample, we find a median of $\Delta M \approx 0.12 M_{\odot}$, as the initial MEarth sample was constructed to be limited to only the mid-to-late M dwarfs.

4. Detecting Brown Dwarfs with Microlens Parallax - Jennifer C. Yee

Microlensing is not normally associated with brown dwarf discoveries. Most of the focus of microlensing has been on exoplanets, so the events that receive the most attention are those due to a two-body lens with a mass ratio $q = M_2/M_1 \lesssim 10^{-3}$. This ignores the vast majority of events, which are due to single "stars" and "stellar" binaries ($q \geq 10^{-2}$). Most of the lenses in these neglected events are M dwarfs, the most common stars. However, because microlensing is a random process, the complete sample of lenses reflects the full, underlying Galactic population, including brown dwarfs. The hard part is identifying which specific microlensing events are created by lenses containing brown dwarfs.

While basic characterization of the target stars is automatic for most planet finding techniques, even determining the masses of the lenses in microlensing events can be difficult because most or all of the observed light comes from the unrelated, background source. Nevertheless, mass measurements for brown dwarf lenses (with typical distances of > 500 pc) are possible if higher-order microlensing effects are observed and the following equation can be solved:

$$M_{\rm Lens} = \frac{\theta_{\rm E}}{\kappa \pi_{\rm E}}, \tag{1}$$

where $\pi_{\rm E}$ is the microlens parallax, $\theta_{\rm E}$ is the angular size of the Einstein ring, and $\kappa = 8.14\,{\rm mas}\,{\rm M}_{\odot}^{-1}$.

The microlens parallax ($\pi_{\rm E}$) is the trigonometric relative parallax between the source and lens ($\pi_{\rm rel}$) scaled to the angular size of the Einstein ring ($\theta_{\rm E}$):

$$\pi_{\rm E} = \frac{\pi_{\rm rel}}{\theta_{\rm E}}. \tag{2}$$

Parallax effects can be observed because the exact form of the microlensing light curve depends sensitively on the *apparent* alignment of the source and the lens projected onto the plane of the sky. When a microlensing event is observed from multiple locations, the different lines-of-sight from the different locations can give rise to measurably different light curves, an effect called terrestrial parallax (see Figure 1 of Gould et al. 2009). In addition, orbital parallax due to the Earth's motion can measurably distort the light curve (see Figure 1 of Gould & Horne 2013). Measuring either or both of these effects gives a measurement of $\pi_{\rm E}$, half the necessary information to solve for the lens mass.

The other half of the information, $\theta_{\rm E}$, can be measured if finite source effects are observed, an effect which takes advantage of the fact that the source is a star with a finite size

Table .1: Examples of brown dwarfs identified from microlens parallax and finite source effects.

Event Name	Mass Ratio q	Primary ($M_\odot$)	Secondary ($M_\odot$)	Reference
OGLE-2007-BLG-224	...	0.056	(none)	Gould et al. (2009)
OGLE-2009-BLG-151/ MOA-2009-BLG-232	0.42	0.018	0.0075	Choi et al. (2013)
MOA-2010-BLG-073	0.0654	0.16	0.010	Street et al. (2013)
MOA-2011-BLG-104/ OGLE-2011-BLG-0172	0.121	0.18	0.02	Shin et al. (2012)
MOA-2011-BLG-149	0.134	0.14	0.019	Shin et al. (2012)
OGLE-2011-BLG-0420	0.377	0.025	0.0094	Choi et al. (2013)
OGLE-2013-BLG-0102	0.13	0.082	0.011	Jung et al. (2014)

rather than a theoretically perfect point source. The observed magnification of the source star is the integration of the magnification pattern across its face. If the source crosses over a caustic, a point or curve with zero width where the magnification diverges to infinity, the time it takes the source to cross this feature ($t_\star$) is measurable from the light curve. Comparing $t_\star$ to the time it takes for the source to cross the Einstein ring (t_E) gives a measurement of the source size:

$$\rho = \frac{t_\star}{t_\mathrm{E}} = \frac{\theta_\star}{\theta_\mathrm{E}} \tag{3}$$

where $\theta_\star$ is the intrinsic angular size of the source. The position of the source on the color-magnitude diagram combined with surface brightness relations (e.g., Kervella et al. 2004) gives a measurement of $\theta_\star$ and hence, θ_E. *Most quantities in microlensing are measured relative to the size of the Einstein ring. Hence, in order to measure θ_E, one must measure a quantity whose intrinsic angular size is known.*

Combining the microlens parallax and finite source effects gives a measurement of the lens mass, which is used to identify lenses containing brown dwarfs. Table .1 gives some examples of microlensing brown dwarfs identified using these techniques. It includes an isolated brown dwarf (Gould et al. 2009), brown dwarf companions to stars (Shin et al. 2012; Street et al. 2013), and close (< 1 AU) brown-dwarf/brown-dwarf binaries (Choi et al. 2013; Jung et al. 2014). Figure 5 of Jung et al. (2014) compares some of these very, low-mass binaries to other low-mass binaries.

In the future, we can expect more brown dwarf discoveries from ongoing and upcoming microlensing surveys. Furthermore, the number of mass measurements (and brown dwarf discoveries) can be increased by increasing the number of parallax measurements made. The simplest method is to use satellite parallax, which is analogous to terrestrial parallax but uses a spacecraft such as *Kepler* or *Spitzer* as the second observatory (Gould 1994; Dong et al. 2007; Gould & Horne 2013). Simultaneous observations from the ground and space give a longer physical baseline than for terrestrial parallax, leading to more pronounced effects in the resulting light curves.

Finally note that while this discussion focuses on brown dwarfs, these techniques are broadly applicable to measuring masses with microlensing and, among other things, can be used to identify free-floating planets and isolated, stellar mass black holes.

5. SPIRou, a nIR Spectropolarimeter / High-Precision Velocimeter at CFHT - Jean-Francois Donati & Julien Morin

SPIRou is a near-infrared (nIR) spectropolarimeter and high-precision velocimeter currently in construction for the Canada-France-Hawaii Telescope (CFHT). SPIRou is optimized for two high-impact science topics, (i) the quest for habitable Earth-like planets around low-mass stars, and (ii) the study of low-mass star and planet formation in the presence of magnetic fields. SPIRou will be able to tackle many more science programs, from weather patterns of brown dwarfs to Solar-system-planet and exoplanet atmospheres, dynamo processes in fully-convective bodies, planet habitability and massive star formation. Planned for a first light at CFHT in 2017, SPIRou is ideally phased for coordinated observations of exoplanets, protostars and protoplanetary systems with other major space and ground facilities like JWST, TESS, CHEOPS, ALMA and, later-on, PLATO. Technically speaking, SPIRou will cover a wide simultaneous nIR spectral domain (0.98-2.35 μm, i.e., YJHK bands) at a resolving power of 73.5K and provide polarimetric capabilities, with a 15% average throughput and a radial velocity (RV) precision of 1 m/s. Both the K band and the polarimetric capabilities are key assets for the two main science goals. A copy of SPIRou for the ESO NTT is currently under study. More general information about SPIRou can be found in Delfosse et al. (2013).

With an extended survey of $\simeq$600 nearby M dwarfs, SPIRou is expected to detect $\simeq$300 super Earths – $\simeq$50 of which located within the habitable zone (HZ) of their host stars. Thanks to its spectropolarimetric capabilities and high Zeeman sensitivity, SPIRou will be able to probe the magnetic topologies of all targeted M dwarfs while measuring their RV curves at the same time – allowing one to work out novel techniques for filtering out the activity jitter from RV curves (e.g., Hébrard et al 2014, in press), for improving the precision of RV measurements and/or for extending RV studies to more active late M dwarfs. SPIRou will also carry out a large survey of $\simeq$250 low-mass protostars in $\simeq$5 of the nearest star-forming regions aimed at studying magnetic fields of protostars, their origin, their evolution with time and their impact on star and planet formation – thus amplifying the pioneering surveys currently carried out with optical instruments (e.g., Donati et al. 2013). By combining spectropolarimetry with high-precision RV, SPIRou will be able to clean RV curves of disc-less protostars from most of their activity jitter (Donati et al 2014, in press, see also Fig. .3), thus giving the opportunity to look for hot Jupiters around protostars and to quantitatively assess the role of disc-migration in the formation of close-in giant planets.

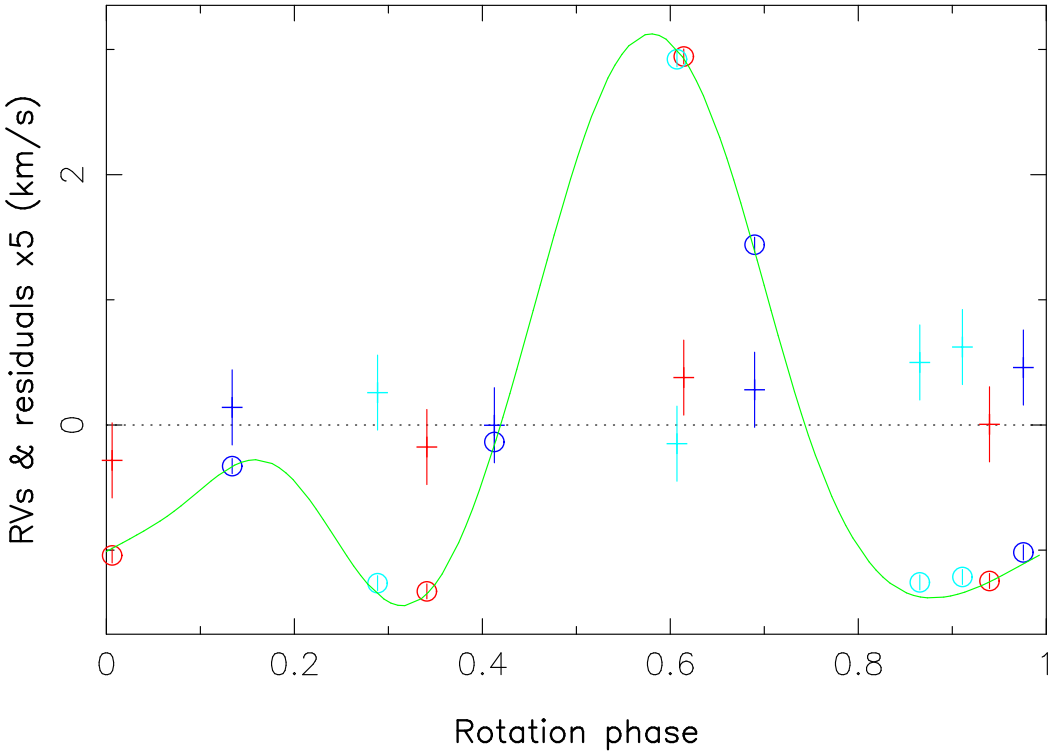

Figure .3: RV variations of the disc-less protostar LkCa 4 as a function of rotation phase, as measured from our observations (open circles) and predicted by the filtering technique described in Donati et al 2014 (green line). RV residuals (expanded by a factor of 5 for clarity), are also shown (pluses) and exhibit a rms dispersion equal to 0.055 km/s, i.e., 78× smaller than the full amplitude of RV variations (of 4.3 km/s). Red, dark-blue and light-blue symbols depict measurements secured at rotation cycles 0, 2 and 3 respectively.

6. Near-Infrared Radial Velocities From Hundreds of Kepler Eclipsing Binaries and Exoplanet Host Stars With APOGEE - Scott W. Fleming[3]

Combining precise photometric and spectroscopic data of detached eclipsing binaries (EBs) can be used to derive masses and radii of the stellar components to a few percent. At this level, the derived masses and radii can be used to constrain new models of stellar structure. One active area of research involves observed radii of stars that are larger than model predictions. This effect is largely seen for stars with masses $< 0.8\,M_{\odot}$. However, the sample of EBs with high-precision measurements is largely underpopulated at low masses and long periods. The APOGEE instrument on the SDSS 2.5m telescope offers an efficient means of surveying large areas of the Kepler field with moderately precise radial velocities

[3]with R. Deshpande (PSU), Chad F. Bender (PSU), Suvrath Mahadevan (PSU), Gal Matijevîc (Villanova), Robert C. Marchwinski (PSU), Kyle Conroy (Vanderbilt), Leslie Hebb (HWS), Hasan Ak (Erciyes), Joshua Pepper (Lehigh), Duy Cuong Nguyen (Toronto), Nathan De Lee (NKU), Andrej Prša (Villanova)

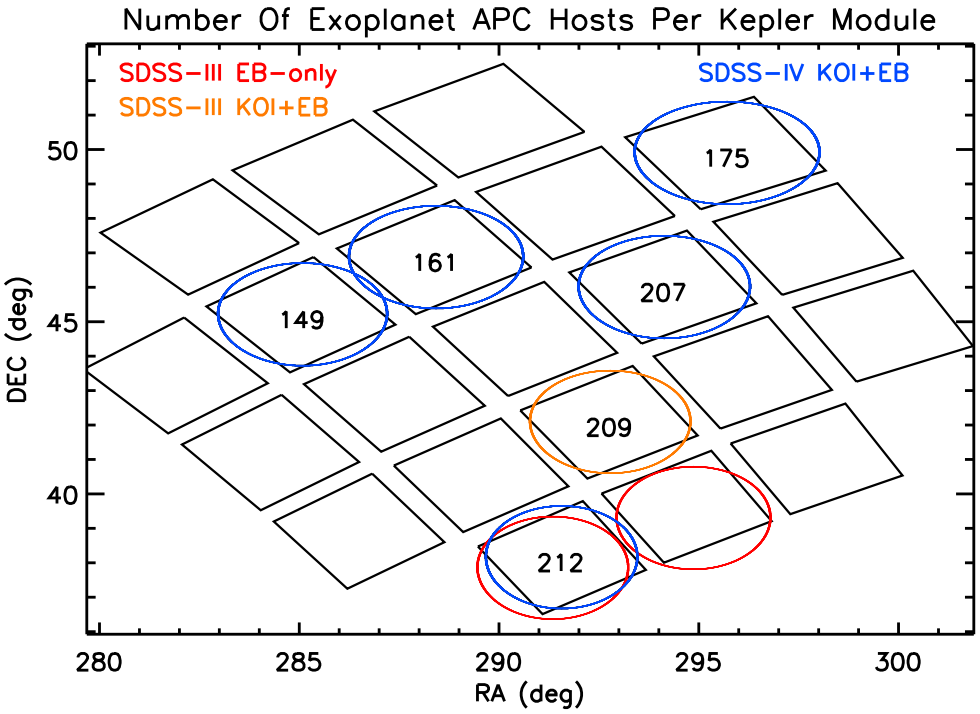

Figure .4: Location of our EB and KOI fields within SDSS-III and SDSS-IV. A total of 159 Kepler detached EBs will be observed, while the number of active planet candidates we observe are shown within each SDSS footprint (circles). The Kepler modules are the square footprints.

(RVs). The instrument is a high resolution (22500), near-infrared (H-band), multi-object (230 science targets), RV-stable (100-200 m/s) spectrograph ideal for studying Kepler EBs. We can derive masses and radii at the few percent level, even for F/G + K/M EBs that are part of our sample. Our sample also includes pairs of stars with mass ratios close to unity (to within 1-2%). Such mass "twins" also provide a useful testbed for stellar internal structure, since any observed differences in radii or effective temperature in stars with essentially the same mass attest to the component interactions that change stellar evolution mechanisms. Beyond studying known EBs, the instrument is capable of studying Kepler planet host stars en masse thanks to its multiplexing capability. APOGEE can robustly identify false positive transiting planets due to physical stellar companions, while those that remain viable candidates can be searched for long-period, non-transiting companions and have the host star abundances derived for over a dozen elements.

6.1 Eclipsing Binaries With APOGEE

We have observed 109 EBs from the catalogs of Slawson et al. (2011) and Prša et al. (2011) as part of APOGEE (Allende Prieto et al. 2008) ancillary programs within SDSS-III (Eisenstein et al. 2011). The targets are chosen in two APOGEE fields that overlap with the Kepler modules containing NGC 6791 and NGC 6819, although few if any of our targets are cluster members themselves (red footprints in Fig. .4). By design, the target selection imposes a

minimum amount of selection cuts in order to explore as diverse a range of stellar and orbital properties as possible. We only choose targets that are classified as having a detached morphology in the EB catalogs, and that have $H < 13$. A total of three and six epochs are observed for the two fields, respectively. Additional Kepler EBs will be observed during SDSS-IV (each with a total of 18 epochs). We supplement the SDSS-III APOGEE observations with optical spectra taken with the High Resolution Spectrograph on the Hobby-Eberly Telescope (Tull 1998). Although we have been able to derive double-line spectroscopic solutions of high contrast systems before (e.g., the Kepler-16 circumbinary planet host system; Bender et al. 2012), the flux ratio for EBs composed of solar-like primaries and low-mass secondaries is an order of magnitude better in the H band. Such systems are particularly well-suited for studying the mass-radius relationship, since the primaries have (comparatively) well-understood, mostly-radiative atmospheres that agree well with current models.

The Mass-Radius Relationship Of Low-Mass EBs

As an example of APOGEE's capability to measure precise, double-lined spectroscopic RVs, even for systems with optical flux ratios as low as 1%, we present two systems that are amongst the first results from our program (Mahadevan et al. 2014). The first (Fig. .5, left) is composed of a $1.2\,M_{\odot}$ F dwarf primary and a $0.5\,M_{\odot}$ M dwarf secondary. After modeling the RVs and Kepler lightcurves using the PHOEBE (Prša & Zwitter 2005) software package, we run a Markov Chain Monte Carlo to derive the posterior distributions of all parameters, and ultimately, uncertainties for the stellar masses and radii. For this system, we achieve relative precisions of 1% for the masses and radii. The second system is composed of a $0.8\,M_{\odot}$ K dwarf primary and a $0.23\,M_{\odot}$ M dwarf secondary. We achieve relative mass precisions of 7% and 4%, respectively, and radii precisions of 2%. These two EBs populate undersampled regions of parameter space along two axes: first, three out of the four components have masses below $0.8\,M_{\odot}$, and second, both these EBs have long periods ($P > 5$ days).

Equal-Mass Stellar Twins

Another test of stellar models can be performed using EBs whose components have mass ratios of unity. Such systems are expected from binary formation models (Simon & Obbie 2009), but only a few percent of a large sample of EBs will have mass ratios within 1% of each other. Fortunately, the Kepler EB catalog is large enough to contain a population of such systems. Fig. .6 shows one such system from our sample: a pair of F dwarfs with a mass ratio $q = 0.996 \pm 0.003\,M_{\odot}$. Since the stars have such similar masses, any differences between their other properties (radii, effective temperatures, rotation rates, surface features, abundances), even at minor levels, can be significant constraints to models of their internal structure and atmospheres.

6.2 Kepler Exoplanet False Positives With APOGEE

Kepler EBs are excellent stellar laboratories for testing the mass-radius relationship, but they are also a common false positive source for transiting exoplanets. Several scenarios exist where an EB has its true eclipse depth diluted by a factor that makes it consistent with a transiting planet-sized object. The high-precision RVs and multiplexing capacity of APOGEE allows for a survey of Kepler Active Planet Candidates (APCs). Our program targets several hundred APCs across five different Kepler modules (Fig. .4, orange and blue footprints) in SDSS-III and SDSS-IV. False positive planet candidates caused by diluted,

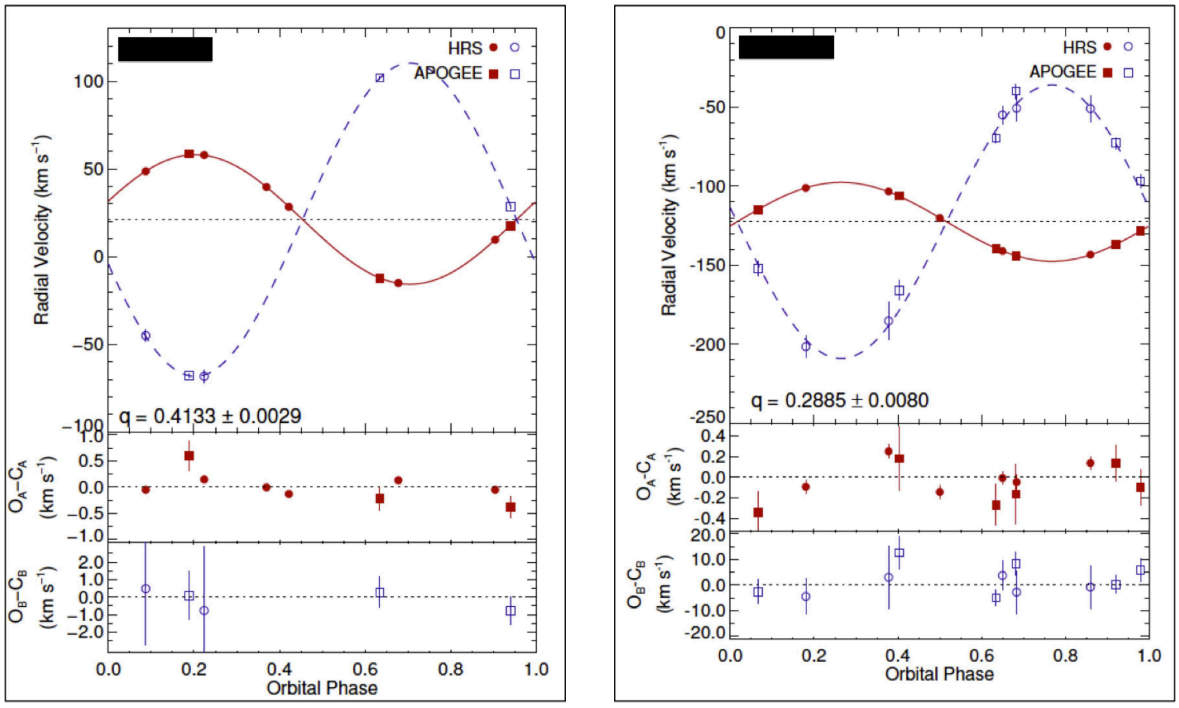

Figure .5: Two EBs from our SDSS-III sample. The one on the left is composed of a 1.2 $M_\odot$ + 0.5 $M_\odot$ pair (masses and radii to 1%), while the one on the right is composed of a 0.8 $M_\odot$ + 0.2 $M_\odot$ pair (radii to 3%, masses to 7% and 4%).

physically-bound stellar binaries can be identified through the cross-correlation function (CCF) with a stellar template. In many cases the two components will be well-separated, and a complete orbital solution can be obtained with a dozen or more observations. In other cases, the spectra are blended even at APOGEE's resolution, but a careful examination of the CCF shape mapped to the ephemeris information reported by Kepler can be used to identify particularly insidious false positives (Fig. .7). Those planet candidates that do not show such large variations are prime targets for further ground-based observations at higher RV precision. Meanwhile, the APOGEE RVs can be used to probe for longer-period, non-transiting companions to study the multiplicity of Kepler planetary systems. Finally, the coadded APOGEE spectra can be used to derive abundances for over a dozen elements using the APOGEE Stellar Parameters and Chemical Abundance Pipeline (ASPCAP, Garcia Perez et al. 2014), opening another dimension in which to explore the Kepler planets as a population.

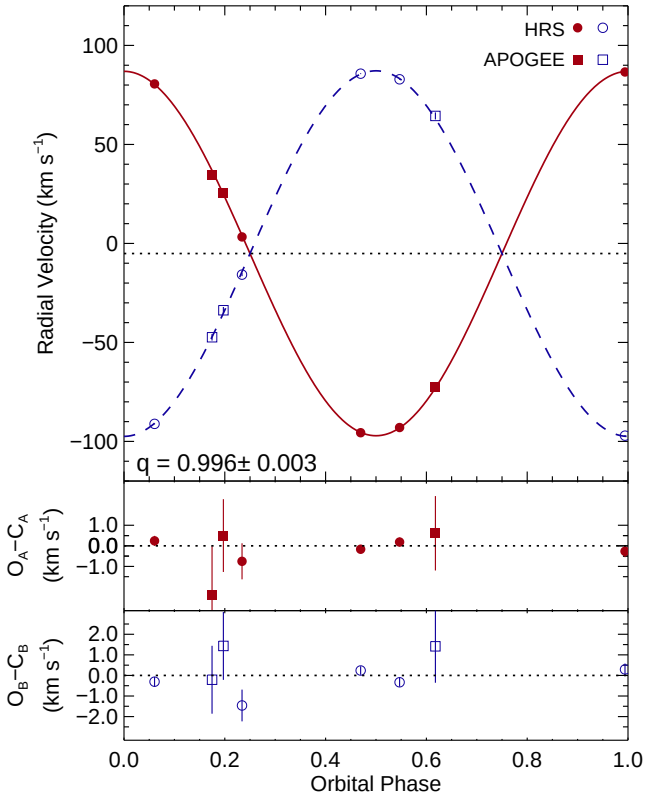

Figure .6: Example of a "mass twin" with mass ratio $q = 0.996 \pm 0.003\,M_\odot$. Such systems offer important model constraints in their own right.

7. Solar Like Activity of the TrES-2 Host Star? - Stefanie Raetz[4]

TrES-2 is one of few exoplanets, which offer the matchless possibility to combine long-term ground-based observations with continuous satellite data. Because of the nearly continuous observations of the Kepler space telescopes for a duration of 4 years, TrES-2 is one of the photometrically best studied transiting exoplanets. We analyzed seven years of ground based observations along with data of 18 observation quarters (Q0- Q17) of the Kepler space telescope. Altogether 491 individual transit mid-times were obtained. The long observation period allowed a very precise redetermination of the transit ephemeris. Owing to unprecedented precision of Kepler we determined the system parameters independently for each of the 435 Kepler transits and searched for any variations. We found no statistically significant change in the orbital inclination i and the transit duration D, but the radius ratio $k = \frac{r_\mathrm{b}}{r_\mathrm{A}}$, hence the transit depth, shows a slight increase which is significant with $3.2\,\sigma$. This finding could be an indication of an increasing stellar activity. The translation from the increasing

[4]with T.O.B. Schmidt (Hamburger Sternwarte), G. Maciejewski (NCU Toruń), R. Neuhäuser (AIU Jena)

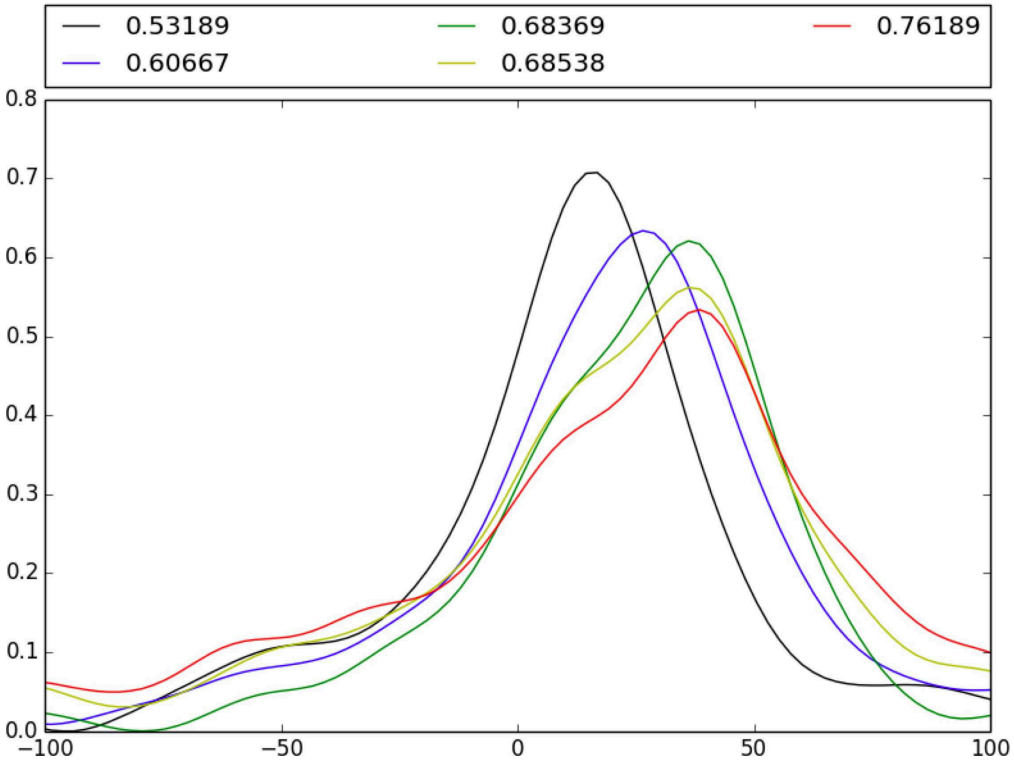

Figure .7: Example of a partially blended APOGEE cross-correlation function of an active Kepler planet candidate. The x-axis is radial velocity in km s^{-1}, the y-axis is CCF power, and the color of each CCF corresponds to the orbital phase of the purported planet based on the Kepler exoplanet catalog. Since the two components are nicely phased to the Kepler ephemeris, this system is likely a false positive planet.

transit depth to a change in spot coverage yielded a value of 0.44% which seems to be plausible compared to the solar cycle. Hence, we probably found, for the first time, solar like activity on a transiting planet host star by analyzing transit events.

7.1 Introduction

The hot Jupiter TrES-2 (P$\sim$2.47 days) was first discovered by O'Donovan et al. (2006). Photometric and spectroscopic follow-up observations were done by Holman et al. (2007), Sozzetti et al. (2007), Ammler-von Eiff et al. (2009), and Winn et al. (2008b). TrES-2 is in the field of view of the *Kepler* space telescope, making it one of the photometrically best studied transiting exoplanets.

There have been controversial discussions about a changing orbital inclination in the TrES-2-system. Mislis & Schmitt (2009) argued that the transit duration has shortened since 2006 by about $\sim$3.16 min, indicating a decrease of the orbital inclination. Rabus et al. (2009) do not confirm this trend. New observations by Mislis et al. (2010) showed again a decrease of the inclination. But the analysis of Scuderi et al. (2010) showed only a non significant change. Additional transits of the NASA EPOXI mission of Christiansen et al. (2011) weakened the

claims of the decreasing inclination further. The analysis of data from the *Kepler* space telescope by Gilliland et al. (2010) and Kipping & Bakos (2011) (quarters 0 and 1) finally ruled out a change of the inclination as a function of time on the level predicted by Mislis & Schmitt (2009). However, by modelling the transits of four observation quarters of *Kepler* Schröter et al. (2012) found a marginally significant positive slope of $\Delta i = (8 \pm 2) \times 10^{-5}$ °/cycle which could be a hint for systematic variations. Daemgen et al. (2009) detected a companion candidate with a projected separation of $1.089 \pm 0.009''$ to the TrES-2 host star in high resolution images obtained with the *AstraLux* Lucky Imaging camera of the Calar Alto Observatory. With a magnitude difference in the z'-band of 3.43 mag with respect to the TrES-2 host star the companion candidate contaminates the photometric data, which leads to systematic errors in the light curve analysis (,,third light").

We observed TrES-2 at the University Observatory Jena since 2007. The results are published in Raetz et al. (2009), Raetz et al. (2011), and Raetz et al. (2014). Here we describe the analysis of 435 transits from 18 quarters of *Kepler* data.

7.2 *Kepler* data

For our analysis we used *Kepler* data of quarters Q0 to Q17. The data were downloaded from the "NASA Exoplanet Archive" (Akeson et al. 2013) which provides fully reduced photometric time-series. The used light curves were generated with the "Kepler Data Processing Pipeline" (Jenkins et al. 2010; Fanelli et al. 2011). We downloaded the fully processed ("Presearch Data Conditioning Simple Aperture Photometry", PDCSAP) data (Twicken et al. 2010). The *Kepler* light curves cover an observation period from May 2nd, 2009 to May 11th, 2013 and included a total of 435 transits. TrES-2 was observed in short cadence mode.

7.3 Light curve analysis

For the calculation of a synthetic light curve we used the JKTEBOP code (Southworth et al. 2004a,b). The main parameters are the orbital period P, the mid-transit time T_c, the orbital inclination i and the radii of star and planet expressed in relation to the semi-major axis a (fractional radii):

$$r_A = \frac{R_A}{a}, \qquad r_b = \frac{R_b}{a}$$

where R_A, R_b correspond to the absolute radii of star and planet respectively. To avoid parameter correlations, JKTEBOP uses parameter combinations such as the sum of the fractional radii ($r_A + r_b$) and the radius ratio $k = \frac{r_b}{r_A}$, instead of fitting r_A and r_b directly. Each light curve was modelled individually.

To determine parameter errors we applied two different methods: Monte Carlo (MC) simulations and a residual permutations algorithm ("prayer bead", Jenkins et al. 2002) to account for red noise. We always adopted the maximum of the MC and prayer bead errors as the final uncertainties. For the analysis of the *Kepler* data we approximated the best fitting model with JKTEBOP for each of the 435 individual transits. All parameters were set free except of the LD coefficients, which were determined before by fitting a phase-folded and binned light curve consisting of 84 transits (Q0-Q3), and the contribution of the third light which was fixed to the value of Southworth (2011).

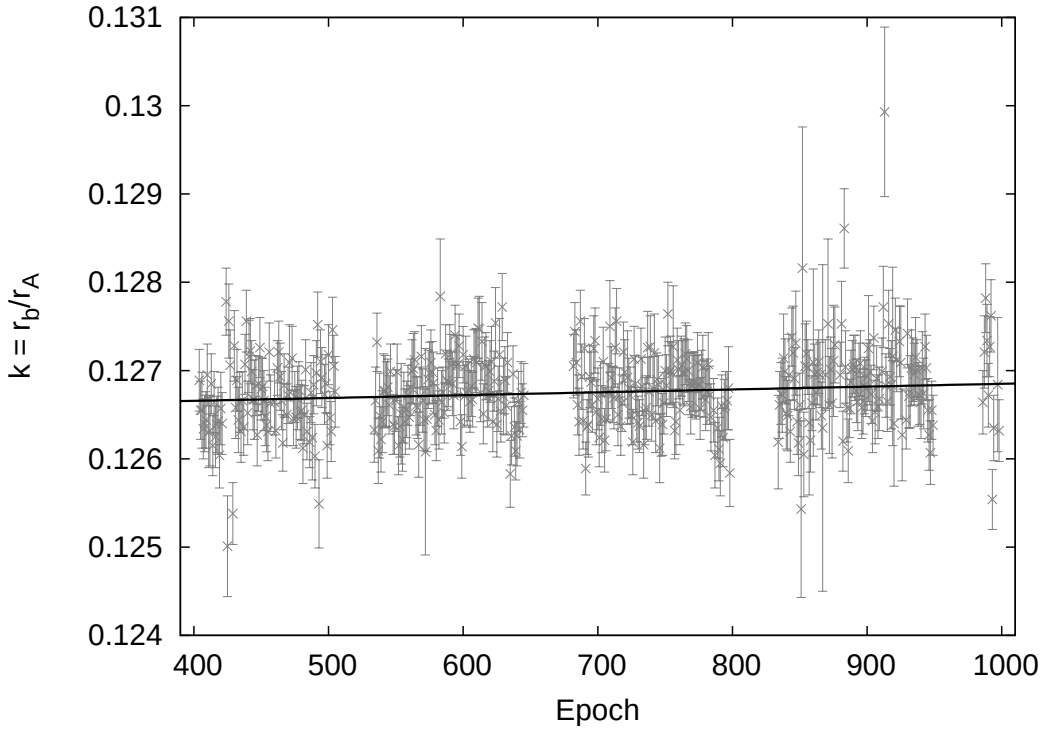

Figure .8: Radius ratio k versus epoch for all 435 *Kepler* transits. The black line represents the best weighted linear fit.

7.4 Variation in system parameters

For each transit the system parameters were determined independently to search for any variation. For each parameter, we did a weighted linear regression. While the analysis of Schröter et al. (2012) yields a slight inclination increase of $\Delta i = (8 \pm 2) \cdot 10^{-5}$ °/epoch, we could not confirm their result. With our larger data set we found a value of $\Delta i = (0 \pm 1) \cdot 10^{-5}$ °/epoch which is consistent with zero. Since the larger timespan of 4 years gives tighter constraints on any variation we found no evidence of an increasing inclination.

For the sum of the fractional radii our analysis yields similar results as for the orbital inclination. The fit gave a value of $\Delta(r_\mathrm{A} + r_\mathrm{b}) = (1 \pm 2) \cdot 10^{-7}$ 1/epoch, meaning that no deviation from zero is noticeable. Only the radius ratio, hence the transit depth, shows an increase of $\Delta k = (3.2 \pm 1.0) \cdot 10^{-7}$ 1/epoch. This result is significant with $3.2\,\sigma$. To test if we can reproduce this result we repeated the calculation after a $2\,\sigma$-clipping. The weighted linear fit of the remaining 384 points yielded a slightly lower slope of $\Delta k = (2.7 \pm 1.1) \cdot 10^{-7}$ 1/epoch which is still significant with $2.5\,\sigma$. To account for a possible underestimation of the uncertainties the error bars where rescaled with a so-called β factor (Winn et al. 2008a). We calculated the β factor for all 435 *Kepler* light curves. This analysis yielded an average of $\beta = 1.08 \pm 0.09$. After rescaling the error bars the positive slope is still significant with $2.9\,\sigma$. Therefore a slight increase of the radius ratio seems to be evident.

7.5 Discussion

An increase of the radius ratio k means either an increase of the fractional planetary radius $r_{\rm b}$ or a decrease of the fractional stellar radius $r_{\rm A}$. As we do not know a mechanism that could drive the increase of fractional planetary radius so fast (within the 4 years of *Kepler* data), it is more likely that stellar activity i.e. stellar spots could be responsible for changes of the average temperature, hence the effective stellar radius. The positive trend in k translates into a decreasing luminosity of 0.28%. This was transferred into a change of spot covered area of 0.44% assuming a constant stellar radius and a spot temperature of 4500K (compared to the temperature of 5795K of the G0V star). Note, that no spot signature could be found in the *Kepler* transit light curves.

We compared our result to the 11 yr solar cycle. Foukal et al. (2006) determined the variation amplitude of the solar constant within the last three solar cycles to $\sim 0.90\,Wm^{-2}$. If translated to luminosity this yields a variation of 0.066% (change of spot coverage 0.1%). However, the last 3 solar cycles lie within the modern maximum. If we also consider the Maunder Minimum the luminosity variation can be as high as 0.2% (change of spot coverage 0.34%) (Lean 2000) which is comparable to the value of the TrES-2 host star. However, the Sun is known to be a magnetic very inactive star i.e. it is near the bottom of the distribution of variability of solar-like stars (Radick et al. 1998). This means that it is likely that the TrES-2 host star could have a higher spot covered area. From spectroscopic observations Sozzetti et al. (2007) found a chromospheric emission ratio of $\langle log\, R'_{HK}\rangle = -5.16 \pm 0.15$. This value implies a very low activity of the TrES-2 host star. However, the used spectra were taken in 2006 and would not disagree with a changing stellar activity. The Ca II H & K activity index for the TrES-2 host star of $\langle log\, R'_{HK}\rangle = -4.949$ found by Knutson et al. (2010) also strengthen the claim of an rising stellar activity.

The increasing activity of the host star should be also visible in the light curve as a brightness decrease of 0.3%. However, the data they used have been quarterly normalized. Hence any trend on time scales longer than 90 days has been removed. The instrumental setup (the rotation of *Kepler* in every quarter) and the consequential systematics make it impossible to find the trend on the expected level in the unnormalized light curve. As there is no sign of stellar activity and rotation in the light curve, the long-term changes in spot coverage seem to be a plausible explanation. To test the hypothesis it is necessary to spectroscopically and photometrically monitor TrES-2 and its host star for the next years to decades.

8. MASCARA, the Multi-site All-Sky CAmeRA - Anna-Lea Lesage[5]

MASCARA, the Multi-site All-Sky CAmeRA, consists of several fully-automated stations distributed across the globe. Its goal is to find exoplanets transiting the brightest stars, in the $m_V = 4$ to 8 magnitude range, currently probed neither by space- nor by ground-based surveys. The nearby transiting planet systems that MASCARA is expected to discover will be key targets for future detailed planet atmosphere observations and characterisations. MASCARA is expected to detect mostly hot Jupiters during its life-time. Thus, the main

[5]with Julien Spronck (Leiden Observatory) and Ignas Snellen (Leiden Observatory)

requirement set on MASCARA to detect these planets around stars down to magnitude 8 is to reach a minimum Signal-to-Noise Ratio of 100 within one hour of observation.

Each MASCARA station consists of five off-the-shelf CCD cameras, fitted with standard wide-field Canon lenses, monitoring the near-entire sky down to magnitude 8 at that location. Measurements have demonstrated that the required Signal-to-Noise Ratio of 100 can be achieved in less than thirty minutes even at the faint end of MASCARA's magnitude range. MASCARA aims at deploying several stations world-wide to provide a nearly continuous coverage of the dark sky, at sub-minute cadence.

While at the faint end MASCARA is limited mainly by photon noise, at the bright end scintillation and red noise become the limiting factors. Instrumental noise sources are reduced by placing the cameras in a fixed orientation and in a temperature controlled environment. By defocusing and allowing stars to drift over the detector, the impact of pixel-to-pixel variations on the photometry are minimized, while taking exposures at fixed sidereal times allows accurate cross-calibration of consecutive nights. In order to minimize data transport and data storage requirements, the raw images are reduced to produce accurate light curves in nearly real time.

The first MASCARA station will be integrated on La Palma in the summer of 2014. MASCARA test data was taken in July 2013 with one camera targeting the transiting exoplanet HD 189733b(Bouchy et al 2005). With a brightness of $m_V = 7.7$, is close to the faint end of the MASCARA magnitude range. Nevertheless, the transit of HD 189733b was successfully detected with $10 - \sigma$ confidence, assuring MASCARA's ability to detect potential transiting planet even at its faint end.

Finally, upcoming spaceborn missions like TESS(Rickers et al 2014) (Transiting Exoplanet Survey Satellite) will complement MASCARA. TESS is NASA's mission to monitor the whole-sky for bright stars. Most of MASCARA targets will be observed by TESS too. Yet, while TESS will probe sky region for about 30 days, MASCARA will have a couple of years coverage by then. Potential TESS candidates could be verified in MASCARA data, and vice-versa.

9. A New Kinematically Unbiased Search for Young, Nearby Stars - Alexander Binks

Samples of coeval stars in nearby, young groups offer a unique opportunity to further our observational constraints on the physics of stellar evolution on the pre-main-sequence. To date at least nine such groups have been unveiled, hosting several hundred stars. Low-mass stars in these groups are particularly interesting as they provide the best conditions for directly detecting sub-stellar companions and can act as a probe for surrounding disk material. The majority of recent search mechanisms to observe low-mass counterparts in these groups have focused on proper-motion selected surveys. These have been successful in terms of finding new members of known groups, but inherently preclude the discovery of new moving groups.

In this talk I present an alternative method, capable of identifying not only members of known moving groups, but also new groups themselves. By cross-correlating objects observed to have short rotation periods in the SuperWASP All Sky Survey with highly active X-ray sources in the ROSAT catalog, optical spectra of a sub-sample of 168 candidates were obtained to assess their youth and kinematics. Using lithium as the primary youth indicator,

further strengthened by gyrochronology, H-alpha emission and rotation periods, 26 stars of spectral type FGK were measured to have ages younger than 100 Myr. Radial velocities and photometric parallaxes for these objects reveal a sub-sample of 11 targets which are tentatively close in their kinematics to the recently identified Octans-Near group. Whether these are members of Octans-Near or not, there nevertheless exists a sub-grouping of several stars with no connection to any previously determined nearby young moving group.

Acknowledgements. Rojas-Ayala acknowledges support from the Fundação para a Ciência e a Tecnologia (FCT) through the Fellowship SFRH/BPD/87776/2012.
Binks: I would like to take this opportunity to express my thanks towards the organising committee of Cool Stars 18 for providing me with the opportunity to present this work.
Dittmann: We gratefully acknowledge funding for the MEarth Project from the David and Lucile Packard Fellowship for Science and Engineering and from the National Science Foundation (NSF) under grant numbers AST-0807690 and AST-1109468. The MEarth team is grateful to the staff at the Fred Lawrence Whipple Observatory for their efforts in construction and maintenance of the facility and would like to thank W. Peters, T. Groner, K. Erdman-Myres, G. Alegria, R. Harris, B. Hutchins, D. Martina, D. Jankovsky, T. Welsh, R. Hyne, M. Calkins, P. Berlind, and G. Esquerdo for their support. This research has made use of NASA's Astrophysics Data System.
Raetz: GM acknowledge the financial support from the Polish Ministry of Science and Higher Education through the Iuventus Plus grant IP2011 031971. RN, and GM would like to thank the European Union in the Framework Programme FP6 Marie Curie Transfer of Knowledge project MTKD-CT-2006-042514 for support. RN would like to thank the German National Science Foundation (Deutsche Forschungsgemeinschaft, DFG) for general support in various projects.

References

Akeson, R. L., Chen, X., Ciardi, D., et al. 2013, ArXiv e-prints

Allende Prieto, C., Majewski, S. R., Schiavon, R., et al. 2008, Astronomische Nachrichten, 329, 1018

Ammler-von Eiff, M., Santos, N. C., Sousa, S. G., et al. 2009, A&A, 507, 523

Bayless, A. J. & Orosz, J. A. 2006, ApJ, 651, 1155

Bender, C. F., Mahadevan, S., Deshpande, R., et al. 2012, ApJ, 751, L31

Bouchy, F., Udry, S., Mayor, M., Moutou, C. Pont, F., Inbarnes, N., da Silva, R., Ilovaisky, S., Queloz, D., Santos, N.-C., Segransan, D., and Zucker, S. 2005, AAP, 444, L15-L19

Choi, J.-Y., Han, C., Udalski, A., et al. 2013, ApJ, 768, 129

Christiansen, J. L., Ballard, S., Charbonneau, D., et al. 2011, ApJ, 726, 94

Daemgen, S., Hormuth, F., Brandner, W., et al. 2009, A&A, 498, 567

Delfosse, X., Donati, J.-F., Kouach, D., et al. 2013, in SF2A-2013: Proceedings of the Annual meeting of the French Society of Astronomy and Astrophysics, ed. L. Cambresy, F. Martins, E. Nuss, & A. Palacios, 497–508

Delfosse, X., Forveille, T., Ségransan, D., et al. 2000, A&A, 364, 217

Dittmann, J. A., Irwin, J. M., Charbonneau, D., & Berta-Thompson, Z. K. 2014, ApJ, 784, 156

Donati, J.-F., Gregory, S. G., Alencar, S. H. P., et al. 2013, MNRAS, 436, 881

Dong, S., Udalski, A., Gould, A., et al. 2007, ApJ, 664, 862

Eisenstein, D. J., Weinberg, D. H., Agol, E., et al. 2011, AJ, 142, 72

Fanelli, M. N., Jenkins, J. M., Bryson, S. T., et al. 2011, Data Processing Handbook, kSCI-19081-001

Foukal, P., Fröhlich, C., Spruit, H., & Wigley, T. M. L. 2006, *Nature* , 443, 161

Garcia Perez, A. E., et al. 2014, in prep

Gilliland, R. L., Jenkins, J. M., Borucki, W. J., et al. 2010, ApJ, 713, L160

Gould, A. 1994, ApJ, 421, L75

Gould, A. & Horne, K. 2013, ApJ, 779, L28

Gould, A., Udalski, A., Monard, B., et al. 2009, ApJ, 698, L147

Holman, M. J., Winn, J. N., Latham, D. W., et al. 2007, ApJ, 664, 1185

Jenkins, J. M., Caldwell, D. A., & Borucki, W. J. 2002, ApJ, 564, 495

Jenkins, J. M., Caldwell, D. A., Chandrasekaran, H., et al. 2010, ApJ, 713, L87

Jung, Y. K., Udalski, A., Sumi, T., et al. 2014, ArXiv e-prints

Kervella, P., Thévenin, F., Di Folco, E., & Ségransan, D. 2004, A&A, 426, 297

Kipping, D. & Bakos, G. 2011, ApJ, 733, 36

Knutson, H. A., Howard, A. W., & Isaacson, H. 2010, ApJ, 720, 1569

Lean, J. 2000, Geophysics Research Letters, 27, 2425

Lépine, S. 2005, AJ, 130, 1680

Mahadevan, S., Bender, C., Deshpande, R., et al. 2014, in prep

Mislis, D. & Schmitt, J. H. M. M. 2009, A&A, 500, L45

Mislis, D., Schröter, S., Schmitt, J. H. M. M., Cordes, O., & Reif, K. 2010, A&A, 510, A107

Nutzman, P. & Charbonneau, D. 2008, PASP, 120, 317

O'Donovan, F. T., Charbonneau, D., Mandushev, G., et al. 2006, ApJ, 651, L61

Prša, A., & Zwitter, T. 2005, ApJ, 628, 426

Prša, A., Batalha, N., Slawson, R. W., et al. 2011, AJ, 141, 83

Rabus, M., Deeg, H. J., Alonso, R., Belmonte, J. A., & Almenara, J. M. 2009, A&A, 508, 1011

Radick, R. R., Lockwood, G. W., Skiff, B. A., & Baliunas, S. L. 1998, ApJS, 118, 239

Raetz, S., Maciejewski, G., Ginski, C., et al. 2014, MNRAS, accepted 2014 July 24

Raetz, S., Maciejewski, G., Mugrauer, M., et al. 2011, in European Physical Journal Web of Conferences, Vol. 11, European Physical Journal Web of Conferences, 5007

Raetz, S., Mugrauer, M., Schmidt, T. O. B., et al. 2009, Astronomische Nachrichten, 330, 459

Rickers, G.R and al, 2014, SPIE Proceedings, 9143-83

Schröter, S., Schmitt, J. H. M. M., & Müller, H. M. 2012, A&A, 539, A97

Scuderi, L. J., Dittmann, J. A., Males, J. R., Green, E. M., & Close, L. M. 2010, ApJ, 714, 462

Shin, I.-G., Han, C., Gould, A., et al. 2012, ApJ, 760, 116

Simon, M., & Obbie, R. C. 2009, AJ, 137, 3442

Slawson, R. W., Prša, A., Welsh, W. F., et al. 2011, AJ, 142, 160

Southworth, J. 2011, MNRAS, 417, 2166

Southworth, J., Maxted, P. F. L., & Smalley, B. 2004a, MNRAS, 349, 547

Southworth, J., Maxted, P. F. L., & Smalley, B. 2004b, MNRAS, 351, 1277

Sozzetti, A., Torres, G., Charbonneau, D., et al. 2007, ApJ, 664, 1190

Street, R. A., Choi, J.-Y., Tsapras, Y., et al. 2013, ApJ, 763, 67

Tull, R. G. 1998, Society of Photo-Optical Instrumentation Engineers (SPIE) Conference Series, 3355, 387

Twicken, J. D., Chandrasekaran, H., Jenkins, J. M., et al. 2010, in Society of Photo-Optical Instrumentation Engineers (SPIE) Conference Series, Vol. 7740, Society of Photo-Optical Instrumentation Engineers (SPIE) Conference Series

Winn, J. N., Holman, M. J., Torres, G., et al. 2008a, ApJ, 683, 1076

Winn, J. N., Johnson, J. A., Narita, N., et al. 2008b, ApJ, 682, 1283